Diffusion of Ultra High Energy Protons in Galaxy Clusters and Secondary X and Gamma Ray Emissions

Corentin Rordorf[1,2], Dario Grasso[2] and Klaus Dolag[3]

[1] *Ecole Polytechnique Federale de Lausanne, Switzerland*
[2] *Scuola Normale Superiore and I.N.F.N., Pisa, Italy*
[3] *Dipartimento di Astronomia, Università di Padova, Padua, Italy*

Abstract

In this work we simulate the propagation of Ultra High Energy (UHE) protons in the magnetised intergalactic medium of Galaxy Clusters (GCs). Differently from previous works on the subject, we trace proton trajectories in configurations of the Intra Cluster Magnetic Field (ICMF) which have been extracted from a constrained Magnetic-SPH simulation of the local universe. Such an approach allows us to take into account the effects of several features of the ICMFs, e.g. irregular geometrical structure and field fluctuations due to merger shocks, which cannot be investigated analitically or with usual numerical simulations. Furthermore, we are able to simulate a set of clusters which have properties quite similar to those of GCs observed in the nearby universe. We estimate the time that UHE protons take to get out of the clusters and found that in the energy range $5 \times 10^{18} \lesssim E \lesssim 3 \times 10^{19}$ eV proton propagation takes place in the Bohm scattering diffusion regime passing smoothly to a small pitch angle diffusion regime at larger energies. We apply our results to estimate the secondary gamma and Hard X Ray (HXR) emissions produced by UHE protons in a rich GC. We show that the main emission channel is due to the synchrotron HXR radiation of secondary electrons originated by proton photo-pair production scattering onto the CMB. This process may give rise to a detectable signal if a relatively powerful AGN, or a dead quasar, accelerating protons at UHEs is harboured by a rich GC in the local universe.

PACS: 98.65Cw, 98.70Sa, 98.70Qy, 98.70Rz

1 Introduction

Several arguments suggest that Galaxy Clusters (GCs) may harbour sources of Ultra High Energy Cosmic Rays (UHECRs). If UHECRs are produced by sources located in the galaxies, e.g. compact stellar remnants or relativistic shocks produced by stellar collapse, these sources will be abundant in GCs which contains hundreds or thousands of galaxies. Active Galactic Nuclei (AGN), which are among the most promising source of UHECRs [1], are typically harboured by elliptical galaxies which are more frequently observed in GC's. Furthermore, GCs may act themselves as accelerators of cosmic rays up to ultra high energies due to the presence of large scale magnetic fields and shock waves produced during the cluster hierarchical accretion [2].

GCs are permeated by a magnetised plasma of electrons and baryons. The density of the Intra Cluster Medium (ICM) is determined by the observation of the X-ray bremsstrahlung emission of the gravitationally heated electron gas. The inferred density is $n_{\rm gas} \sim 10^{-3}$ cm^{-3} which amounts to an over-density of about one thousand with respect to the Inter Galactic Medium (IGM). The presence of Intra Cluster Magnetic Fields (ICMFs) is testified by the extended radio halos due to the synchrotron emission of relativistic electrons in the ICM. The strength of the ICMFs can be estimated from the intensity of the observed radio emission either assuming the minimum energy condition, giving $< B > \sim 0.1 - 1$ μG [3] ($< B > \sim 0.4$ μG for Coma [4]) or by an independent determination of the relativistic electrons density. For a few clusters (especially for Coma) this is made possible by the observation of a HXR emission that, if interpreted as the outcome of Inverse Compton Scattering (ICS) of the relativistic electrons onto the CMB photons, implies the ICMF strength to be in the range $0.2 - 0.4\mu$G [5, 6] However, the interpretation of the HXR radiation from GCs in terms of ICS is still controversial and other models have been proposed which may allow/require stronger ICMF (see e.g. [7, 8, 9]) . Indeed, Faraday Rotation Measurements (RMs) of polarised radio sources placed within the cluster, or in the background, provide significant evidence for the presence of stronger ICMFs in the range $1 - 10$ μG or higher [10, 11]. Furthermore, RMs provide valuable information about the spatial structure of the field which is patchy with coherence lengths in the range between 10 and 100 kpc. It is unclear if the discrepancy between the IGMF strength inferred from the radio halo intensity and that determined from RMs can be explained by the different

sensitivity of these two kind of measurements to the presence of magnetic substructures (for a discussion about this issue and a comprehensive review of IGMF observations see [12]). Interestingly, a recent analysis [13] of BeppoSAX data on the HXR emission from Coma points to a ICMF strength in that cluster which is stronger ($< B > \sim 1$ μG) than the value previously claimed in [5] and it is almost compatible with that inferred from RMs. In the following we will assume that the actual strength of IGMFs is that inferred from RMs.

The magnetised ICM can affect significantly the propagation of cosmic rays up to ultra high energies. The Larmor radius of protons in the ICMFs is smaller than the field coherence length up ultra high energies so that the residence time in a GC can be considerably increased respect to the straight propagation. The effect is even more pronounced for composite nuclei which have a smaller Larmor radius. Here we will focus on the case of protons. At low energies the propagation UHE protons is expected to take place in the spatial diffusion regime. Since diffusion arises due to the scattering of charged particles onto the field irregularities, the diffusion time is expected to depend significantly on the ICMF power spectrum. Although very interesting approaches have been recently proposed to determine the ICMF power spectrum from high resolution RMs [14, 15], so far this is a poorly known quantity. The common attitude is to assume a Kolmogorov power spectrum. Although this is the most natural choice in the case of fully developed, homogeneous turbulence of Navier-Stokes type (no-magnetic) we should take in mind that some, or any, of these conditions may not be fulfilled in the ICM. Indeed, the ICMF power spectrum may depend on the cluster accretion history. Furthermore, cluster merging is expected to compress and twist locally the ICMF giving rise to non-Gaussian MF fluctuations which are non accounted for in conventional CR diffusion simulations which use a synthetic MF with Gaussian fluctuations. The only way to account for the effects of all these ICMF features on the propagation of UHECRs is by means of numerical simulations of the MF large scale structure. Numerical simulations are also mandatory to simulate CR diffusion when the Larmor radius is of the same order of the MF coherence length. We will show that this is the case for protons with energy around 10^{19} eV, i.e. the most interesting energy range for the extensive air shower (EAS) experiments. Furthermore the determination of the diffusion coefficients can be performed analytically only for MF in a regime of weak turbulence. We will show that this may not

be the case for ICMFs.

The main aim of this paper is to estimate the diffusion time of UHE protons in rich GCs as a function of their energy. Differently from previous works on the subject we approach this problem by means of numerical simulations to determine both the ICMF structure of nearby GCs and to trace proton propagation. We extract the ICMF in several GCs from a constrained simulation of the MF structure in the local universe [16] based on the Magnetic Smoothed Particle Hydrodynamics (MSPH) technique developed by Dolag et al. [17]. This simulation traces the passive evolution of the magnetic field in a spherical region of radius 115 Mpc about the Local Group starting from a primordial seed field. It was showed [16, 17] that the simulation reproduces the observed RMs with good accuracy. The main advantage of this approach is that it provides a realistic simulation of the gas and of magnetic field spatial distribution in a number of nearby clusters. It was found that on average the ICMF traces the gas density and it is locally amplified in regions where accretion shocks fronts are present. The ICMF power spectrum has been determined down to the spatial resolution length which is ~ 10 kpc in the cluster center. Significant deviations were found in some GCs respect to a Kolmogorov spectrum. The effects produced by all these features of the ICMF onto the UHECR diffusion can be relevant and were not considered in the existing literature. Our approach allows to take them into account.

As an application of our results we estimate the flux of HXR and gamma rays produced by the interaction of UHE protons with the gas and the radiation within GCs. We will mainly focus on the synchrotron emission of ultra-relativistic secondary electrons, produced by *pp*-scattering, which falls in the GeV region, and by proton photo-pair scattering onto the CMB falling in the HXR region of the electromagnetic spectrum. Whereas the former emission can hardly be detectable, the latter may be detectable if a relatively bright UHE proton source is harboured by a rich GC in the local supercluster.

In Sec. 2 we give a brief description of the MSPH simulation and of the ICMF properties obtained from this simulation. In Sec. 3 we describe our ray-tracing code and the UHE proton diffusion properties at different energies and radii. In Sec. 4 we show that the insertion of MHD turbulence at low length scales, which is unresolved in the MSPH simulation, does not affect significantly our results. In Sec. 5 we compare our approach with that followed by other authors. In Sec. 6 we estimate the secondary gamma-ray emission due to hadronic scattering onto the intra-cluster gas and the HXR

radiation due to the synchrotron emission of electrons and positrons generated by proton photo-pair production scattering. Finally, Sec. 7 contains our conclusions.

2 MSPH simulations and ICMF properties

The origin of ICMFs is still unknown. Although the observed high metallicity of the ICM suggests that it may have undergone a significant pollution driven by galactic winds , the strong intensity of ICMFs, their huge extension (exceeding few Mpc's in some cases), and their large coherence length ($10 \div 100$ kpc's) make hard to explain their origin uniquely by galactic ejection. Another possibility is that ICMFs were generated starting from a seed which is subsequently amplified by the adiabatic compression and the shear flows of the gas driven by the hierarchical accretion of the clusters. Several mechanism have been proposed to explain the origin of the required seed field. For example, it could be ejected by AGN [19], or from a violent starburst activity at high redshift [20], it could be produced by some non-equilibrium process in the early universe [18], or be the result of a Biermann battery [21]. In principle, the battery has the advantage to be independent on unknown physics at high redshift since, in this case, the seed field is produced by thermoelectric currents powered by the cluster merger shocks. In practice, however, the battery can account only for too weak magnetic seeds [22]. A subsequent turbulent dynamo has to be invoked to increase the field strength enough to initiate a successful MHD amplification. Since this process cannot be simulated on the computer, the final intensity of the magnetic field is quite uncertain and has to be tuned to reproduce the RMs of GCs. Operatively, such an approach is, therefore, similar to assume a seed field of primordial origin.

The simulation that we use here is based on the MSPH method developed in [23]. The code combines the merely gravitational interaction of the dominant dark-matter component with the MHD of the electron-baryon gas. In a previous work [17] it was showed that magnetic seed fields in the range of $(0.2-5)\times 10^{-9}$ G at redshift $z_* \simeq 20$ will be amplified due to the structure formation process and reproduce RM in clusters of galaxies. This corresponds to $B_0 \equiv B(z_*)(1+z_*)^{-2} \simeq (0.05-1)\times 10^{-11}$ G at the present time in the unclustered IGM. It was also demonstrated that the MF amplification process

completely erases any memory of the initial field configuration in high density regions like galaxy clusters. Therefore, we can safely set the coherence length $L_c(z_{\rm in})$ of the initial seed field to be infinite in our simulation.

In the simulation which we use here $B_0 = 10^{-12}$ Gauss. The initial conditions for the DM fluctuations were constructed from the IRAS 1.2-Jy galaxy survey by first smoothing the observed galaxy density field on a scale of 7 Mpc, evolving it linearly back in time, and then using it as a Gaussian constraint for an otherwise random realization of the ΛCDM cosmology. We extended the initial conditions of [24] by adding gas, together with an initial MF. Therefore the simulation at redshift zero represents the large scale mass distribution of our local universe as observed. Some of the prominent halos in the simulations can be identified with observed counterparts with mass and temperature within a factor of two or better. In [24] it is shown, that this simulation matches the observed local universe very well in many aspects. Therefore, such an approach allows to use a simulated set of GCs which have very similar properties to those of GCs observed nearby.

The gravitational force resolution of the simulation is 10 kpc. This maximal resolution is reached in the central region of GCs where the SPH test particles are more dense. The volume filled by the mixture of high resolution dark matter and gas particles is a sphere of radius ~ 115 Mpc (centered on the Milky Way) surrounded by a larger region of low resolution dark matter particles, to get long range tidal forces. The mass of the high resolution gas and dark matter particles thereby is $0.48 \times 10^9 M_\odot/h$ and $3.1 \times 10^9 M_\odot/h$ respectively. Therefore the most massive cluster in our simulation is resolved by nearly one million particles.

For our analysis we used the four most massive clusters within our simulation volume, which includes the halos identified as the Perseus and the Coma cluster. Table 1 summarizes the global properties of these clusters. We determined the gas density and magnetic field profiles for the clusters. On average, the magnetic field profiles follow the density profile in the outer part, whereas in the central region the magnetic field profiles flatten, which is consistent with previous findings. Depending on the cluster and its dynamical state, the slope of the magnetic profile in the outer parts scatters around the slope of the gas density, and also the size of the flatter core region varies. Fig. 1 shows, as an example, the profiles for the halo 2 and the halo 4. For the magnetic field we present the norm as well as the radial and transversal component. It is evident from these plots that the MF structure is basically

Table 1: Cluster number, virial radii, virial mass, emission weighted virial temperature and identification with real clusters (if possible).

#	R_{200}[kpc/h]	$M_{200}[M_\odot/h]$	$T_{\rm Lx}$[keV]	name
1	2421.76	1.60e+15	7.1	-
2	2257.75	1.30e+15	5.6	Perseus
3	1958.90	8.50e+14	4.6	-
4	1885.23	7.57e+14	8.3	Coma

isotropic.

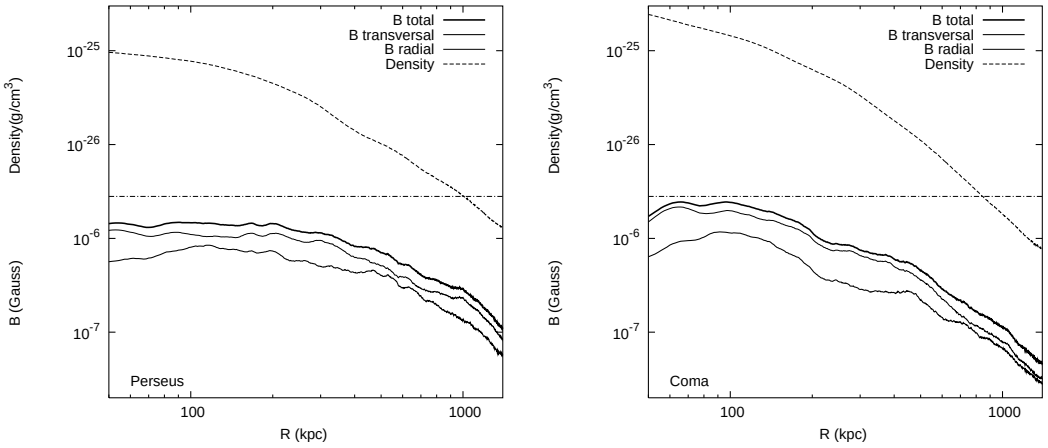

Figure 1: Density and magnetic field radial profiles of clusters 2 and 4. Different spatial components of the ICMF are represented.

We also determined the MF power spectrum $B^2(k)$. As we will discuss in more details in the Sec.3, this quantity is crucial to determine CR diffusion properties in the ICM. We computed $B^2(k)$ by evaluating the MF at the points of a cubic grid. This is done by applying the MSPH formalism to every mesh point of the grid considering all particles which overlap by their smoothing length, taken from the MSPH simulation. Afterwards we performed a FFT (Fast Fourier Transform) on this grid.

In Fig.2 we show the energy spectrum ($B(k)^2k^2$) for clusters 2 and 4. The slope of the power spectrum for the four most massive haloes seems to be

steeper for the more massive ones, but when calculating the spectra for all clusters it looks more likely that it is determined by the dynamical state of the cluster. The spectral index δ ranges between -1.5 and -3 for most of the clusters, with a small number of clusters found to have even more extreme values. On average we found $\delta \simeq -2$ which corresponds to a spectrum slightly steeper than a Kolmogorov's for which (in 3D) $\delta = -5/3$. This is consistent with the results obtained in the first attempts to measure the ICMF power spectra from RM images of extended radio sources ([14, 15]).

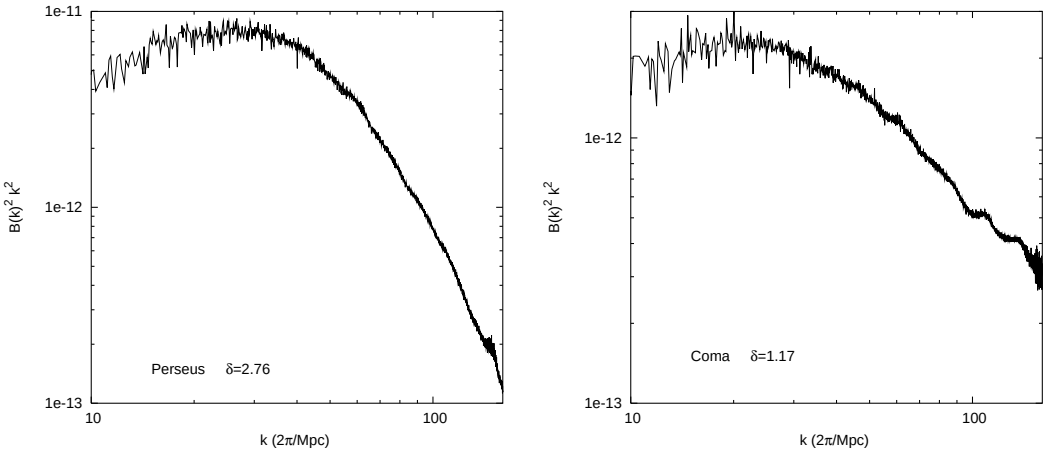

Figure 2: The energy power spectrum is represented for clusters 2 (left) and 4 (right) in arbitrary units. The quoted values of δ represent the best fit to the power law index. $|\delta| = 5/3$ for a Kolmogorov spectrum.

In order to quantify the turbulence strength we define the parameter

$$\eta = \frac{\langle \delta B^2 \rangle}{\langle B^2 \rangle} = \frac{\frac{1}{2\pi^3} \int_{k_{\rm min}}^{k_{\rm max}} dk k^2 B^2(k)}{\int B^2(\mathbf{x}) d^3x} \tag{1}$$

where $k_{\rm min}$ is the wavenumber at which the energy spectrum gets its maximal value and the turbulent cascade sets-in. This is the scale at which most of the MF energy is concentrated. $k_{\rm max}$ is determined by the spatial resolution of the MSPH simulation. Although the physical wavenumber at which dissipation takes place is expected to be much larger, this artificial cut will not affect significantly η due to the rapid decreasing of the turbulent power at small scales.

From the Figs.2 we can estimate $k_{\rm min} \simeq 50\ \frac{2\pi}{\rm kpc}$ almost independently on the cluster mass. We have then a turbulence strength $\eta \simeq 0.6$ over 1 Mpc box. In other words, our MSPH simulation predicts a quite high level of turbulence in rich GCs.

3 Ray tracing and UHE proton distribution in galaxy clusters

We simulate proton trajectories in the synthetic ICMF by solving equation of motion by means of a Runge-Kutta adaptive step size method. Our simulation conserves energy with a very good accuracy: we get $\frac{\delta E}{E} \simeq 10^{-5}$ in the worst case of 10^{18} eV protons over a complete trajectory. As far as it concerns the simulation of proton trajectories, we disregard energy losses. We will verify the validity of this assumption *a posteriori* by comparing the residence time in clusters with the energy loss time due to the relevant collision processes. The ICMF is determined along the proton trajectory by performing a weighted sum (see [23] for details) of the magnetic fields of all smoothed gas particles in the MSPH simulation which overlap with the proton position. In same cases an extra turbulent MF component is artificially added to the result of the simulation to model a possible unresolved, or physically unaccounted, small scale component of the IGMF (see Sec. 5).

In Figs.(3,4) we represent typical proton trajectories in two and three dimensions. These plots clearly show that in the central regions of a rich GC proton propagation takes place in the spatial diffusion regime at energies as large as $\sim 10^{19}$ eV. Several momentum reversals are visible which we interpret to be due to magnetic mirroring onto local enhancements of the magnetic field strength.

We start computing the mean delay time, i.e. the effective arrival time minus the straight propagation time to reach a sphere far out of the cluster (we take it at 35 Mpc radial distance), of 1000 protons injected at the cluster center with energies in the range $10^{18} - 10^{20}$ eV. In Fig.5 we represent the delay time as a function of the proton energy for several GCs. The best fit function is well represented by two power laws with indexes ~ -1 and ~ -2, the knee being located at an energy $E_{\rm cr} \sim (2-3) \times 10^{19}$ eV. In Sec.5 we will argue how this feature corresponds to the protons propagation passing from

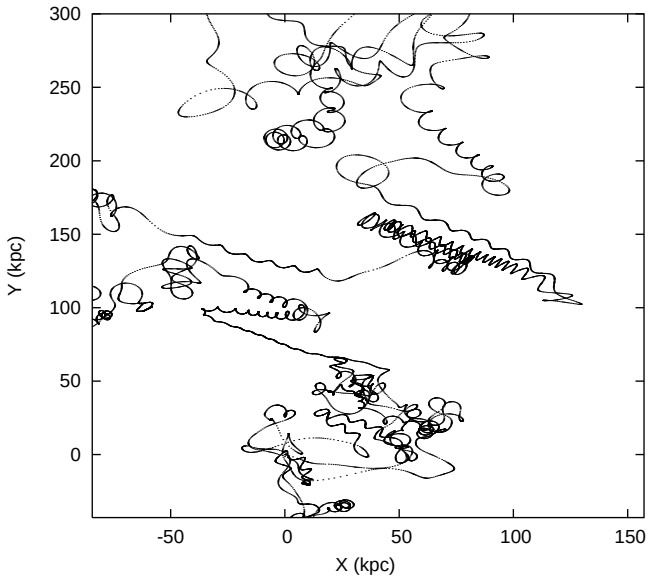

Figure 3: Trajectories of a $E = 5 \times 10^{18}$ eV proton in the central region of cluster 1 projected in 2D.

the spatial diffusion (SD) regime to the small pitch angle (SPA) regime at high energies.

The delay time, that we defined in the above, is representative of the diffusive properties of the entire cluster. In order to get an insight on the radial dependence of this quantity, we computed the delay time from the center up to spheres of different radii. This is represented in the Figs. 6 at several energies for clusters 2 and 4. These plots show that no significant delay is produced at a radius larger than 1 Mpc . Interestingly, this feature is almost independent on the proton energy as it is apparent from the self-similarity of the curves.

Our next step is to compute a set of time intervals t_{ij} representing the mean time that a proton injected in the spherical shell $R_i < R < R_{i+1}$ spend in the shell $R_j < R < R_{j+1}$. Once we specified the injection spectrum and the radial distribution of sources, the knowledge of a sufficiently dense set of

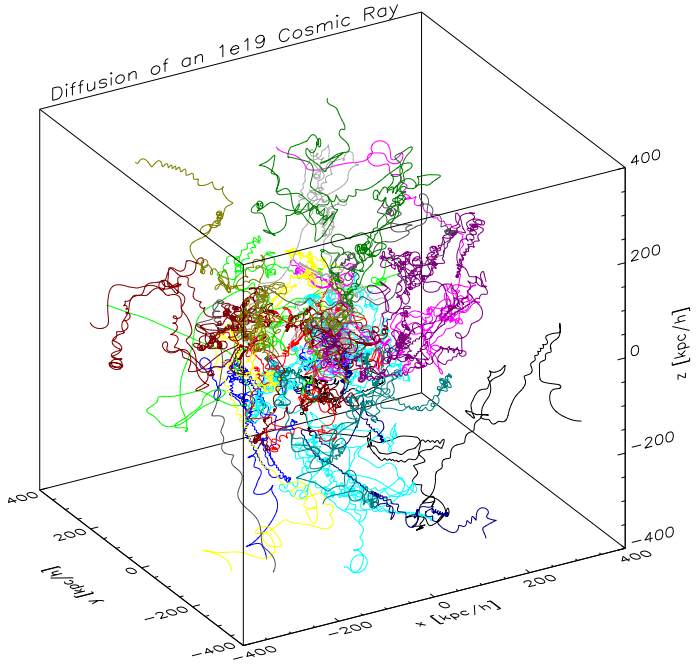

Figure 4: The same of Fig.3 in 3D and for protons with energy 10^{19} eV.

t_{ij} 's allows to determine the differential proton flux at different radii:

$$\frac{dF(E,R_i)}{dE} = Q_s(E)\frac{c}{4\pi}\sum_{j=1}^{m}\frac{(R_{j+1}^3 - R_j^3)}{(R_{i+1}^3 - R_i^3)}\, f\,(R_j)\;\; t_{ij}\;. \qquad (2)$$

Here $f(R_i)$ represents the density of sources and $Q_s(E)$ is the proton injection spectrum of a single source (for the sake of simplicity we assume all the sources to be identical). We took $m = 2000$ corresponding to as many identical shells each of them is 1 kpc thick. The normalization constant A depends on the source injection power. Eq. 2 amounts to a numerical solution of the diffusion equation.

In the case of a point-like single source placed at the center of the cluster, $f(R_i) = \delta_{1j}$, where δ_{ij} is the Kronecker function. It is interesting to plot the histogram of t_{1j}. For a better readability we represent it in Fig.7 in the continuous limit.

In Fig.8 we represent the radial dependence of the proton energy density per logarithmic energy interval at several energies in the case of a single

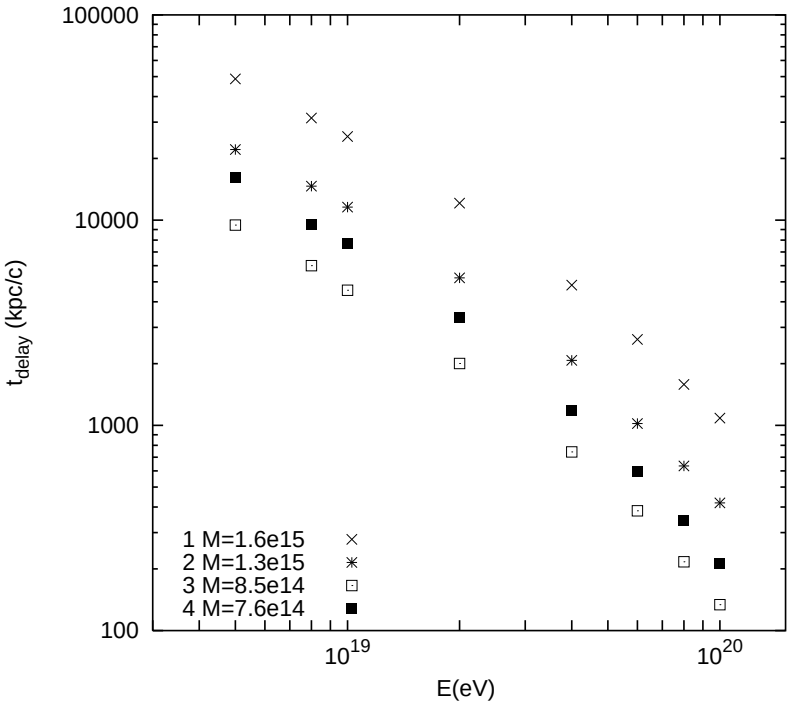

Figure 5: The delay time (residence time within a sphere of radius 0.5 Mpc minus the straight propagation time) for 4 GCs. The quoted GC masses are in solar masse units.

source, with luminosity $L_p(E > 10^{18}\ \mathrm{eV}) = 10^{44}\mathrm{erg\ s}^{-1}$ and spectral index $\alpha = 2$ placed at the center of cluster 4 (Coma).

Another possibility is that the UHECR source distribution traces that of galaxies. We can reasonably assume that the radial distribution of galaxies is well approximated by that of the gas. To be consistent we determine the gas distribution from the result of the MSPH simulation. We found that

$$f(r) = \frac{1}{\left[1+\left(\frac{r}{r_1}\right)^2\right]^{0.51}} \frac{1}{\left[1+\left(\frac{r}{r_2}\right)^2\right]^{0.72}} \frac{1}{\left[1+\left(\frac{r}{r_3}\right)^2\right]^{0.58}} \tag{3}$$

with $r_1 \simeq 10$kpc (spatial resolution limit), $r_2 \simeq 250$ kpc (core radius), $r_3 \simeq 2$ Mpc (virial radius) provides an excellent fit of the simulated gas distribution for GCs with mass $M \sim 10^{15}\ M_\odot$. The mean UHECR luminosity of galaxies

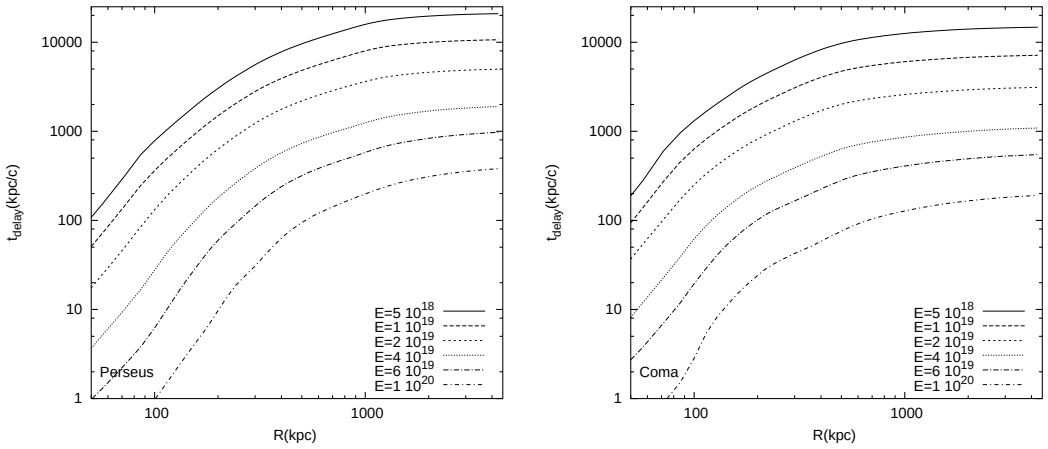

Figure 6: The mean delay time accumulated from the cluster center to the radius R is represented as a function of R for protons of different energies (quoted in eV's) for clusters 2 (left) and 4 (right).

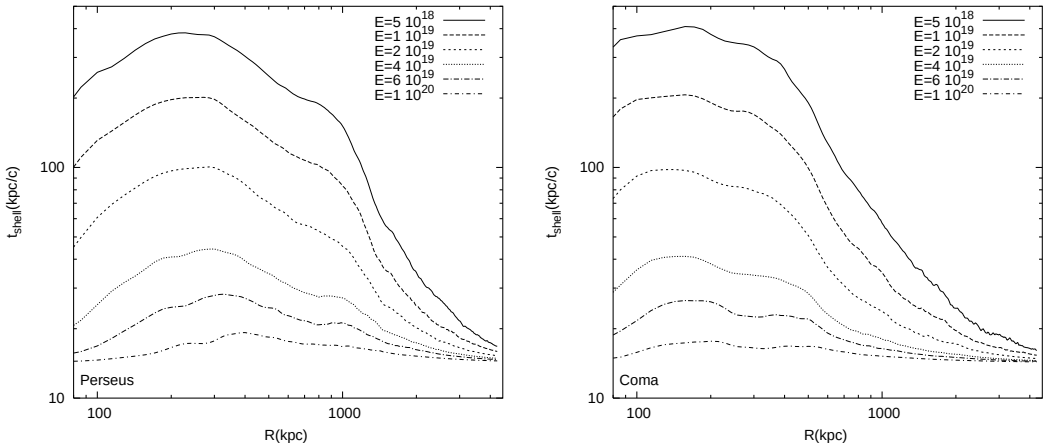

Figure 7: The mean delay time accumulated in spherical shells of thickness 1 kpc and mean radius R for clusters 2 (left) and 4 (right).

can be estimated by assuming that the Milky Way provides a representative sample. The high energy cosmic ray luminosity of our Galaxy have been estimated by several authors, see e.g. [1] where it was found (we assume here that most of the UHECRs are protons $L_p^{\rm gal}(E > 5\times10^{18}\ {\rm eV}) \sim 5\times10^{36}$ erg/s.

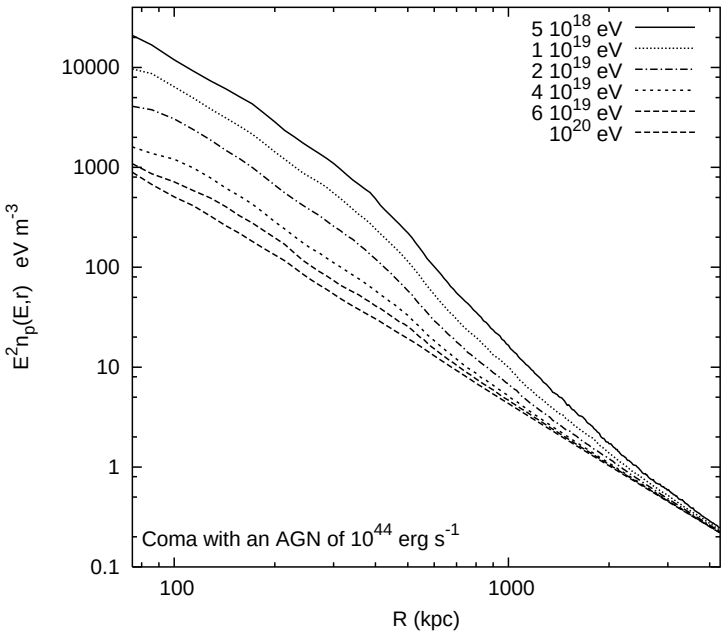

Figure 8: The mean proton energy density in the cluster 4 (Coma) is plotted versus the radial distance from the center for several energies.

Therefore, if the entire luminosity of a rich GC is due to ~ 1000 galaxies, its expected value would be in the range $L_p(E > 5 \times 10^{18}\ \mathrm{eV}) \simeq 10^{39} - 10^{40}$ erg/s. We will show in Sec.6 that this luminosity is too low to give rise to a detectable secondary emission from the ICM.

A similar situation is expected if Gamma Ray Bursts (GRBs) are the main source of UHECRs. One of the main arguments in favour of this hypothesis [25, 26] is the coincidence of the predicted UHECR flux with that observed under the assumption that the energy release under the form of UHECRs by GRBs equals that of gamma rays. The rate of GRBs in a typical galaxy is $\Gamma^{\mathrm{gal}}_{\mathrm{GRB}} \sim 10^{-8}\ \mathrm{year}^{-1}$, hence it is $\Gamma^{\mathrm{GC}}_{\mathrm{GRB}} \sim 10^{-5}\ \mathrm{year}^{-1}$ in a rich GC. Our previous results imply that the diffusion time of UHE nuclei emitted in the central region of a rich cluster ($R \lesssim 1$ Mpc) exceed largely the time interval between GRBs in the cluster. As a consequence, clusters behaves as continuous sources of UHECRs even if elementary sources are GRBs. The

total UHECR luminosity of a galaxy due to GRBs is

$$L_{\rm GRB}^{\rm gal}\left(E > 5\times 10^{18}\ {\rm eV}\right) \sim \Gamma_{\rm GRB}^{\rm gal}\ \left(\frac{E_{\rm GRB}}{10^{52}\ {\rm ergs}}\right) \simeq 10^{36}\ {\rm ergs}^{-1}\ . \qquad (4)$$

This luminosity almost coincide with that previously estimated for UHECRs emitted by galaxies so that, even in this case, we do not expect an observable secondary emission from the ICM.

4 Insertion of synthetic turbulence at small length scale

As we discussed in the above, the maximal resolution of the MSPH simulation is about $2\pi/k_{min} \sim 10$ kpc. This means that the simulation does not account for magnetic fluctuations possibly present below this scale. Beside to the turbulent cascade, MHD turbulence at small scales may be due to a number of effects, e.g. galactic winds and galaxy motion. Since in the central region of GCs the Larmor radius of protons with energy below 10^{19} eV is smaller than the spatial resolution of our simulation, the presence of strong magnetic fluctuations below this scale might spoil the validity of our previous results at low energies.

In order to clarify this issue, we redetermined the delay time in the MSPH magnetic structure of a massive cluster to which we added turbulent MFs at small scale. The extra component of the MF is generated by summing over a large number of randomly distributed plane waves with spherically symmetric direction and with random polarizations and phases. We follow here the approach presented in [27] where it was showed that in the limit of an infinite number of wave modes, the turbulence is isotropic and spatially homogeneous. The modelled turbulent component is given by

$$\delta\mathbf{B}(x,y,z) = \sum_{n=1}^{N_m} A(k_n)\ \hat{\xi}_{\mathbf{n}}\ exp(ik_n z_n' + i\beta_n) \qquad (5)$$

where $A(k_n)$ represents the amplitude of the wave mode with wave number k_n, polarization $\hat{\xi}_n$, and phase β_n. Eq. (5) satisfies $\nabla\mathbf{B}(x,y,z) = 0$. The maximal value of k_n that we used is $2\pi/0.5$ kpc^{-1}. For the sake of simplicity we assume the extra component to have a Kolmogorov spectrum. Since the

MSPH simulation predict a stepper spectrum, we think that this assumption may only lead to overestimate the turbulent power at small scales hence the correction to the delay time.

For generality, we assume the extra turbulent power to have the following radial dependence

$$\frac{\delta \mathbf{B}^2(r)}{\mathbf{B}^2_{\rm MSPH}(r_o)} = \left(\frac{r}{r_o}\right)^{-\alpha} \ . \tag{6}$$

Indeed, it is reasonable to assume that the level of turbulence will be higher in the center of GCs than outside. For example, since the formation of GCs the galaxies at the center make several revolutions around and may then contribute to the level of MHD turbulence. In this case, a resonable choice for r_0 is the cluster core radius $r_0 \sim 500$ kpc. We adopt this choice to compute the delay time of protons versus their energy. This is plotted in Fig.9 for different values of the parameter α. It is evident from this figure that the addition of turbulence at small scales doesn't increase significantly the diffusion time. This means that diffusion properties of protons in the energy range $10^{18} - 10^{20}$ eV are dominated by the MF fluctuations at larger scale, where most of the power is concentrated. Since these fluctuations are well accounted by the MSPH simulation we can reasonably trust the results presented in Sec. 3.

5 Diffusion of UHE protons, comparison with previous results

Diffusion of cosmic rays in disorganised magnetic fields takes place by scattering of the charged particles onto the magnetic irregularities. Particles interact with the field when their gyro-motion resonates with a Fourier component of wavelength equal to the Larmor radius. The diffusion coefficient, defined by $D(E) \equiv \dfrac{\langle \Delta x^2 \rangle}{2\Delta t}$, can be computed analytically in the regime of weak turbulence and for low values of the magnetic rigidity $\rho \equiv 2\pi r_L / L_c \ll 1$. In this case

$$D(E) \simeq \frac{1}{3} r_L c \frac{\langle B^2 \rangle}{\int_{1/r_L}^{\infty} dk B^2(k) k^2} \ , \tag{7}$$

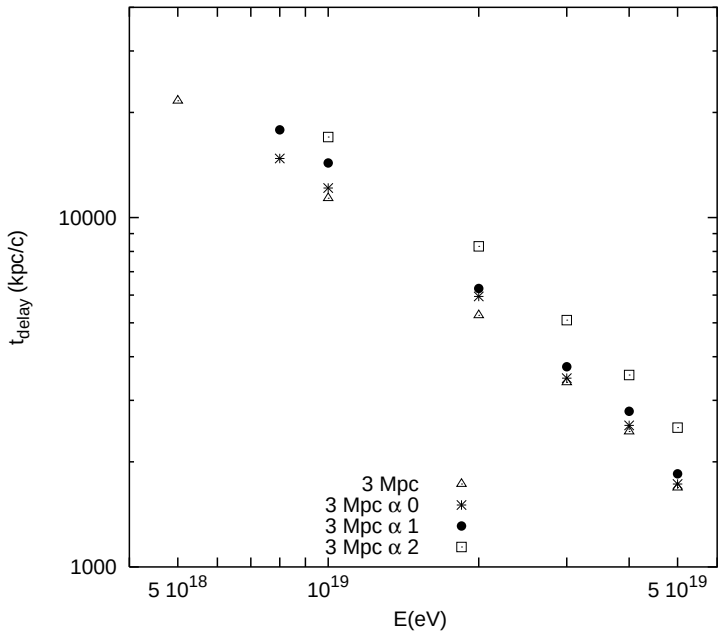

Figure 9: The same as Fig.5 with an extra MHD turbulent power for several values of the parameters r_0 and α defined in Eq.6.

where $B^2(k)k^2$ is the magnetic field energy power spectrum. In the case of a Kolmogorov spectrum, $B^2(k)k^2 \propto k^{-5/3}$, the energy dependence $D(E) \propto E^{-1/3}$ is obtained. A priori there are no reasons why Eq.(7) should hold for UHE protons diffusing in the ICMFs. In Sec. 2 we showed that MSPH predict strong turbulence ($\eta = 0.6$) in the core of rich clusters ($R < 500$ kpc) with a power spectrum which may be significantly steeper than a Kolmogorov's. Furthermore, since the Larmor radius

$$r_L \simeq \frac{E}{ZeB} \simeq 10 \left(\frac{E}{10^{19}\ \mathrm{eV}}\right) \left(\frac{B}{10^{-6}\ \mathrm{G}}\right)^{-1}\ \mathrm{kpc}, \tag{8}$$

is comparable to the field coherence length L_c, the magnetic rigidity of UHE protons in the cluster is quite close to unity.

Numerical simulations of charged particle diffusion have been performed in the case of strong Kolmogorov turbulence [28]. These simulations confirmed the validity of Eq.(7) for low values of the magnetic rigidity. However, significant deviations from the $E^{-1/3}$ behaviour were found when the mag-

netic rigidity approaches unity. The best fit to the numerical results gives (in units of $\mathrm{Mpc}^2/\mathrm{Myr}$):

$$
\begin{aligned}
D(E) &\simeq 0.004 \left(\frac{E}{10^{20}\ \mathrm{eV}}\right)^{1/3} \left(\frac{B}{\mu\mathrm{G}}\right)^{-1/3} \left(\frac{L}{\mathrm{Mpc}}\right)^{-2/3}, \quad E \lesssim 0.1 E_{\mathrm{cr}} \\
D(E) &\simeq 0.03 \left(\frac{E}{10^{20}\ \mathrm{eV}}\right) \left(\frac{B}{\mu G}\right), \qquad 0.1 E_{cr} \lesssim E \lesssim E_{\mathrm{cr}} \\
D(E) &\simeq 0.02 \left(\frac{E}{10^{20}\ \mathrm{eV}}\right)^{7/3} \left(\frac{B}{\mu G}\right) \left(\frac{L}{Mpc}\right)^{-4/3}, \quad E_{\mathrm{cr}} \lesssim E
\end{aligned}
\tag{9}
$$

In these expressions $E = E_{\mathrm{cr}}$ corresponds to the condition $\rho = 1$. Accordingly to these results, the energy dependence of the diffusion time, $t_{\mathrm{diff}}(E) = r^2/6D(E)$, changes rather smoothly from a quasi-rectilinear regime at $E \simeq E_{\mathrm{cr}}$, with $t_{\mathrm{diff}}(E) \propto E^{-7/3}$, to the, so called, Bohm diffusion regime with $t_{\mathrm{diff}}(E) \propto E^{-1}$, for $0.1E_{cr} \lesssim E \lesssim E_{\mathrm{cr}}$. The analytically predicted behaviour, $t_{\mathrm{diff}}(E) \propto E^{-1/3}$, was found only at low energies, $E \lesssim 0.1E_{cr}$.

However, the properties of the magnetic field configuration assumed in [28] are still quite different from those of ICMF given by our MSPH simulation. Indeed, the mean field intensity, which was assumed to be uniform in [28], has a quite pronounced radial profile in all the simulated clusters. Furthermore, MSPH simulations predict a turbulent power spectrum which is often quite different from a Kolmogorov's. We think that these simulation provide a much more realistic picture of the real ICMF configuration.

First of all we checked that our numerical code reproduces the diffusion coefficients found in [28] in the energy range $10^{18} - 10^{20}$ eV for strong homogeneous turbulence. Remarkably, we found that our results are in good agreement with those of [28] also in the case the field configuration is that determined by the MSPH simulation. The energy at which the delay time passes from a $\sim E^{-2}$ dependence, consistently with small pitch angle diffusion, to E^{-1} (Bohm scattering diffusion) is $\sim 3 \times 10^{19}$ eV. This energy corresponds to a Larmor radius of $\sim$ 30kpc, for $\langle B \rangle \simeq 1\ \mu$G, which almost coincide with the scale $L_{min} = 2\pi/k_{min}$ at which we found that most of ICMF energy is concentrated.

6 Hard X and gamma-ray emissions

In this section we apply our previous results to estimate the flux of high energy photons produced by the interaction of UHE protons with the gas and the radiation in the magnetised core of a rich GCs. Such a radiation may provide a signature of the possible presence of powerful UHECR sources in galaxy clusters. For the sake of simplicity we will assume that a GC harbour a single point-like UHE proton source placed at its center. We will only consider the contribution of protons in the energy range $5 \times 10^{18} \lesssim E \lesssim 3 \times 10^{19}$ eV with injection spectrum $n_p(E)dE = E^{-\gamma}dE$ [1].

We start estimating the flux of gamma-rays due to hard hadronic interactions (pp-scattering) of UHE protons with the baryon gas in the ICM. The differential photon production rate $Q_\gamma(E)$ from the decay of secondary π^0's is given by [2]:

$$Q_\gamma(E) \simeq Y_\gamma \, \frac{L_p(E > E_{\rm min})}{E_{\rm min}^2} \left(\frac{E}{E_{\rm min}}\right)^{-\gamma} \sigma_{pp} n_{\rm gas} c t_{\rm diff}(E) \qquad (10)$$

where Y_γ is the fraction of proton energy transferred to the photons and $\sigma_{pp} \simeq 3 \times 10^{-26}$ cm^2 is the pp-scattering cross section (we neglect here a weak energy dependence of this quantity). In Sec.3 we found that, in the energy range $5 \times 10^{18} \lesssim E \lesssim 5 \times 10^{19}$ eV, the diffusion path length of protons in the core of a cluster with mass $\sim 8 \times 10^{14}$ M$_\odot$ (like Coma) is

$$c t_{\rm diff}(E) \simeq 20 \left(\frac{E}{5 \times 10^{18}\ {\rm eV}}\right)^{-1} \ {\rm Mpc} \ . \qquad (11)$$

Therefore the gamma-ray energy emission rate per logarithmic energy interval of the primary protons is

$$E^2 Q_\gamma(E) \simeq 10^{40} \left(\frac{Y_\gamma}{0.1}\right) \left(\frac{n_{\rm gas}}{10^{-3}\ {\rm cm}^{-3}}\right) \left(\frac{L_p\,(E > E_{\rm min})}{10^{44}\ {\rm erg\ s}^{-1}}\right) \left(\frac{E}{E_{\rm min}}\right)^{1-\gamma} {\rm erg\ s}^{-1}, \qquad (12)$$

where $E_{\rm min} = 5 \times 10^{18}$ eV. Since the mean free path of $E_\gamma \sim 10^{19}$ eV photons, due to $\gamma + \gamma_{\rm CMB} \rightarrow e^+ + e^-$, is much smaller than the cluster core radius [29],

[1] By injection spectrum we mean here the spectrum of protons which leave the acceleration region reaching the ICM. This may differ from the acceleration spectrum due to energy losses close to the source.

practically the entire energy of the photons will be converted into electromagnetic showers inside the cluster. The shower, however, cannot escape the cluster. This is promptly understood by comparing the synchrotron energy loss length of the electron-positron component of the shower,

$$l_{\rm syn} \simeq 2 \left(\frac{B}{1\ \mu{\rm G}}\right)^2 \left(\frac{10^{18} eV}{E_e}\right)\ {\rm pc}\ , \tag{13}$$

with the cluster size and the IC scattering length over which electrons and positrons might energise CMB photons, which are much larger. Therefore, all the energy of the photons produced by π^0 decay is converted into synchrotron photons. For monochromatic electrons, and for a uniform magnetic field, the photon synchrotron spectrum would peak at the energy

$$\hbar\omega_{\rm syn} = \frac{3\sqrt{\alpha}B}{2m_e^3}E^2 \simeq 10 \left(\frac{E}{10^{18} eV}\right)^2 \left(\frac{B}{1\ \mu{\rm G}}\right) {\rm GeV} \tag{14}$$

with width $\delta\omega \sim \omega_{\rm syn}$. Secondary electrons (and positrons) from pp-scattering, however, are spread over a range of frequencies which is much larger than $\delta\omega$ so that the spectral shape of the synchrotron emission is mainly determined (we neglect here a possible dependence on the IGMF power spectrum which will be investigate elsewhere) by the electron energy spectrum[30] hence, in turn, by the primary proton spectrum in the cluster.

It is worth noticing here, that the synchrotron emission in the GeV region would be overwhelmed by the secondary emission produced by low energy protons if the UHE protons spectrum extends to lower energies with a power $\gamma \gtrsim 2$. There may be cases, however, in which the proton emission is peaked at ultra high energies (see below about possible scenarios which may give rise to this situation).

If we assume that the proton energy spectrum in the ICM peaks at $E_{\rm max} \sim 10^{19}$ eV the synchrotron emission will peak at an energy of few tens of GeV's. Photons with this energy can travel over cosmological distances without undergoing significant energy losses and might be detectable by the GLAST satellite [31] or the MAGIC Cherenkov telescope [32]. We find, however, that the expected photon flux

$$\dot{n}_\gamma \simeq \frac{1}{E_\gamma}\,\frac{E^2 Q_\gamma(E)}{4\pi d^2} \simeq 3{\times}10^{-13} \left(\frac{L_p\,(E > 5\times 10^{18}\ {\rm eV})}{10^{44}\ {\rm erg\ s^{-1}}}\right) \left(\frac{d}{100\ {\rm Mpc}}\right)^2 {\rm cm}^2 s^{-1} \tag{15}$$

is much lower than the expected sensitivity of these instruments, unless the UHE proton source is extremely bright ($L_p\,(E > 5 \times 10^{18}\ \mathrm{eV}) \gg 10^{46}\ \mathrm{erg\ s^{-1}}$) which, however, may contradict other constraints.

A more promising signature of the presence of a powerful UHE proton source in a GC could be given by the synchrotron emission of secondary electrons and positrons produced by the process $p + \gamma_{CMB} \rightarrow e^+ + e^- + p$ (proton photo-pair production). It is remarkable that, for protons in the energy range $5 \times 10^{18} \lesssim E \lesssim 3 \times 10^{19}$ eV, the secondary electrons produced by this process are practically monochromatic with energy ~ 830 TeV [1]. As a consequence, the spectrum of the synchrotron photons emitted in the cluster peaks in the hard X-ray (HXR) range, around ~ 10 keV (see Eq.14). Interestingly, a non-thermal emission from the Coma cluster, peaking at this energy, has been already detected. The observed energy flux is [5, 13] $E_X^2 f(E_X) \simeq 10^{-11}\ \mathrm{erg\ cm^2 s^{-1}}$. In order to estimate the primary proton flux required to explain this signal in terms of secondary $e^{\pm}$ synchrotron emission we need to know the probability for a proton to undergo photo-pair production scattering inside the cluster. This probability is maximal at $E \sim 10^{19}$ eV, at which it takes the value

$$\mathrm{P_{pair}}(10^{19}\ \mathrm{eV}) = 1 - \exp\left(-\frac{ct_{\mathrm{diff}}(10^{19}\ \mathrm{eV})}{l_{\mathrm{pair}}(10^{19}\ \mathrm{eV})}\right) \simeq 10^{-2}\ , \qquad (16)$$

where we used our Eq. (11) to find the proton diffusion time in the cluster and the interaction length $l_{\mathrm{pair}}(E \sim 10^{19}\ \mathrm{eV}) \simeq 1000$ Mpc determined in [36, 37]. Therefore the UHE proton luminosity required to explain the Coma HXR emission entirely in terms of synchrotron emission of electrons produced by proton pair production scattering is given by

$$L_p\left(E > 5 \times 10^{18}\ \mathrm{eV}\right) = 4\pi d^2\ \mathrm{P_{pair}^{-1}}\ \Phi_X \simeq 10^{45}\ \ \mathrm{erg\ s^{-1}}\ . \qquad (17)$$

This luminosity corresponds to $L_p\,(E > 1\ \mathrm{GeV}) \gtrsim 10^{46}\ \ \mathrm{erg\ s^{-1}}$ for $\gamma \gtrsim 2$, and it increases rapidly for larger values of γ. Even for $\gamma \simeq 2$, the required proton luminosity would be too high to be compatible with the EGRET limit [33] on the secondary gamma-ray emission in the 100 Mev - 10 GeV range due to *pp*-scattering . It would also give rise to a too intense radio synchrotron emission from *pp* secondary electrons [7]. Furthermore, a proton source with luminosity $L_p\,(E > 5 \times 10^{18}\ \mathrm{eV}) > 10^{45}\ \ \mathrm{erg\ s^{-1}}$ may be at odd with the

results of UHECR experiments which, so far, do not show any evidence of a flux excess in the direction of Coma.

A possible way out from some of these problems is to assume a flatter proton spectra in the cluster, i.e. $\gamma < 2$. This may be the case if UHE protons are accelerated in the knots and hot spots of a powerful AGN's jet [34]. Another possibility is that the proton acceleration is not stochastic. Rather, it may be induced by the huge electric field generated by a supermassive rotating black-hole (a so called "dead quasar"). It was showed in [35] that proton energies as large as 5×10^{19} eV can be reached in this case with a quite narrow spectral distribution. Although, a quite intense TeV gamma-ray direct emission is expected from such an object, this emission is predicted to be beamed so that its detection may be missed. In a such a case the X and gamma-ray diffuse emission produced by secondary particles in a GC harbouring the source may offer an independent signature.

Even if the HXR excess from Coma is not due to an intense UHE protons emission in that GC, weaker proton sources may still give rise to a detectable HXR signal from closer GCs. Indeed the expected X-ray flux in the $10 - 100$ keV region due to synchrotron emission of secondary electrons is

$$\Phi_X \simeq 2{\times}10^{-12} \left(\frac{\mathrm{P_{pair}}}{10^{-2}}\right) \left(\frac{d}{20\ \mathrm{Mpc}}\right)^2 \left(\frac{L_p\,(E > 5 \times 10^{18}\ \mathrm{eV})}{10^{43}\ \ \mathrm{erg\ s^{-1}}}\right) \ \ \mathrm{erg\ s^{-1}\ cm^{-2}} \tag{18}$$

A proton luminosity $L_p\,(E > 5 \times 10^{18}\ \mathrm{eV}) \simeq 10^{43}\ \ \mathrm{erg\ s^{-1}}$ corresponds to $L_p\,(E > 1\ \mathrm{GeV}) \simeq 10^{44}\ \ \mathrm{erg\ s^{-1}}$ for $\gamma = 2.1$. This is a standard luminosity for an AGN. The required luminosity can be even smaller if the proton spectrum is peaked at high energies. Therefore an AGN or a dead quasar accelerating protons at UHEs may give rise to a detectable signature under the form of synchrotron HXRs if they are harboured by a rich GC in the local supercluster.

We note on passing, that a mechanism similar to that we just discussed here has been recently considered in [9]. The main difference with our mechanism is that in [9] the synchrotron emitting electron-positron pairs were assumed to be produced by photons with energy $E_\gamma = 700$ TeV. No compelling process was suggested, however, to explain the origin of the required flux of photons with that particular energy.

An independent signature of the presence of a UHE proton bright source may be provided by the secondary gamma ray radiation produced in the

IGM by the protons which escape the clusters. The relevant process at $E \gtrsim 10^{19}$ eV is, again, proton pair-production onto the CMB. If IGMFs are weaker than 10^{-10} G, as it is suggested by the results of the large scale MSPH simulation performed in [16], the electromagnetic showers produced by the secondary electrons and photons can travel over a distance of hundreds Mpc's [38]. For a source at a distance of ~ 20 Mpc the electromagnetic shower at the observer position will be composed by photons, electrons and positrons with energies which can exceed several TeV's. Since the shower production probability is in this case $P_{\rm pair} \sim 2 \times 10^{-2}$, the photon flux around 1 TeV can be roughly estimated to be

$$\dot{n}_\gamma(E_\gamma \sim 1 \text{ TeV}) = \frac{L_p}{4\pi d^2 \, E_\gamma} \mathrm{P}_{\rm pair} \simeq 2{\times}10^{-12} \left(\frac{L_p}{10^{43} \text{ erg s}^{-1}}\right) \left(\frac{d}{20 \text{ Mpc}}\right)^2 \text{cm}^2\text{s}^{-1} \, . \tag{19}$$

Such a flux should not be missed by Cherenkov gamma-ray telescopes like MAGIC [32], HESS [39] and VERITAS [40].

Detailed computations of the expected spectra in the gamma as well as in the HXR region are beyond the aims of this work and they will be presented elsewhere.

7 Conclusions

In this paper we investigated the propagation of UHE protons in the magnetised medium of Galaxy Clusters. By using a constrained MSPH simulation of the magnetic field structure in the local universe we were able to account, for the first time, for several features of the ICMF which we think to be present in actual nearby clusters. We showed that UHE propagation takes place in the spatial diffusion regime in the core of rich GCs ($M \simeq 10^{15} \ M_\odot$) up to the $E_{\rm cr} \simeq 3{\times}10^{19}$ eV. Below this energy, at least down to $\sim 5{\times}10^{18}$ eV, the diffusion time scales with energy like E^{-1} (Bohm scattering diffusion). In spite of the different ICMF power spectrum found in different simulated clusters, we found that the behaviour of the proton residence time as a function of the energy does not changes significantly from cluster to cluster. Only the amount of the delay changes depending on the mean intensity of the ICMF. The path length increase due to the ICMF is too small to give rise to a significant modification of the proton energy spectrum due to energy losses in

the ICM, since $ct_{\rm delay} \sim 10$ Mpc $\ll l_{\rm loss} \sim 10^3$ Mpc for $E \sim 10^{19}$ eV. Since the residence time of UHE protons is much larger than that expected for straight propagation, and for small pitch angle diffusion, the probability for them to undergo hadronic or photo-pair production scattering is considerably increased. In order to determine a possible signature of a bright proton source harboured by a GC, we applied our results to estimate the gamma ray and HXR secondary emission produced by UHE protons in the ICM. We showed that electromagnetic showers produced by *pp*-scattering and proton photo-pair production do not leave the cluster due to the intense synchrotron losses. Therefore, their energy is transferred to synchrotron photons of lower energy which can reach the observer without further losses. The synchrotron gamma-ray emission from the electrons produced by the decay of secondary pions is too weak to be detected. More promising is the synchrotron emission of secondary electrons and positrons produced by proton photo-pair scattering which falls in the HXR range. We showed that the UHE proton emission of a relatively powerful AGN placed in a GC in the local supercluster may give rise to a detectable HXR emission.

Acknowledgments

We would like to thank P. Blasi and M. Vietri for helpful discussions and suggestions. We also thank V. Springel and I. Tkachev for collaboration performing the constrained MSPH simulation which we used in this paper. D.G. thanks Lin Yin for collaboration in the initial phase of this work. K. Dolag acknowledges support by a Marie Curie Fellowship of the European Community program 'Human Potential' under contract number MCFI-2001-01227.

References

[1] V. S. Berezinsky *et al.*, " Astrophysics of Cosmic Rays", North-Holland, Amsterdam, 1990.

[2] V. S. Berezinsky, P. Blasi and V. S. Ptuskin, Astroph. J. **487**, 529 (1997) [arXiv:astro-ph/9609048].

[3] L. Feretti, in "Diffuse thermal and relativistic plasma in galaxy clusters", eds. Bohringer et al. MPE report **271**, 3 (1999).

[4] G. Giovannini *et al.*, Astroph. J. **406**, 399 (1993).

[5] R. Fusco-Femiano *et al.*, Astroph. J. **513**, L21 (1999). [arXiv:astro-ph/9901018].

[6] Y. Rephaeli, J.M. Stone, and P. Blanco, Astroph. J. **511**, 21 (1999).

[7] P. Blasi and S. Colafrancesco, Astropart. Phys. **122** (1999) 169 [arXiv:astro-ph/9905122].

[8] A. M. Atoyan and H. J. Volk, Astrophys. J. **535**, 45 (2000) [arXiv:astro-ph/9912557].

[9] A. N. Timokhin, F. A. Aharonian and A. Y. Neronov, Astron. Astrophys. **417**, 391 (2004) [arXiv:astro-ph/0305149].

[10] L. Feretti *et al.*, Astron. Astrophys. **344**, 472 (1999) [arXiv:astro-ph/9902019].

[11] G. B. Taylor, *et al.*, Mon. Not. Roy. Astron. Soc. **326** (2001) 2 [arXiv:astro-ph/0104223].

[12] C. L. Carilli and G. B. Taylor, Ann. Rev. Astron. Astrophys. **40** (2002) 319 [arXiv:astro-ph/0110655].

[13] R. Fusco-Femiano, *et al.*, Astrophys. J. **602** (2004) L73 [arXiv:astro-ph/0312625].

[14] C. Vogt and T. A. Ensslin, arXiv:astro-ph/0309441.

[15] M. Murgia *et al.*, submitted to Astron. & Astrophys., 2004.

[16] K. Dolag, D. Grasso, V. Springel and I. Tkachev, arXiv:astro-ph/0310902.

[17] K. Dolag, M. Bartelmann and H. Lesch, Astron. & Astrophys. **387**, 383 (2002). arXiv:astro-ph/0202272.

[18] D. Grasso and H. R. Rubinstein, Phys. Rept. **348** (2001) 163 [arXiv:astro-ph/0009061].

[19] S. Furlanetto and A. Loeb, Astrophys. J. **556**, 619 (2001) [arXiv:astro-ph/0102076].

[20] H. J. Volk and A. M. Atoyan, Astrophys. J. **541**, 88 (2000) [arXiv:astro-ph/9812458].

[21] D. Ryu, H. Kang and P. L. Biermann, Astron. & Astrophys. **335**, 19 (1998).

[22] R. M. Kulsrud, R. Cen, J. P. Ostriker and D. Ryu, Astrophys. J. **480**, 481 (1997) [arXiv:astro-ph/9607141].

[23] K. Dolag, M. Bartelmann and H. Lesch, arXiv:astro-ph/9906329.

[24] H. Mathis et al., MNRAS, **333**, 739 (2002).

[25] E. Waxman, Phys. Rev. Lett. **75** (1995) 386 [arXiv:astro-ph/9505082].

[26] M. Vietri, Astrophys. J. **453** (1995) 883 [arXiv:astro-ph/9506081].

[27] J .Giacalone and J.R. Jokipii Astrophys. J. **520**, 204 (1999).

[28] F. Casse, M. Lemoine and G. Pelletier, Phys. Rev. D **65** (2002) 023002 [arXiv:astro-ph/0109223].

[29] R. J. Protheroe and P. L. Biermann, Astropart. Phys. **6** (1996) 45 [Erratum-ibid. **7** (1997) 181] [arXiv:astro-ph/9605119].

[30] M. S. Longair, "High Energy Astrophysics", Cambrigde Press 1994.

[31] GLAST: http://glast.gsfc.nasa.gov/

[32] MAGIC: http://hegra1.mppmu.mpg.de/MAGICWeb/

[33] P. Sreekumar *et al.*, Astrophys. J. **464**, 628 (1996).

[34] F. A. Aharonian, Mon. Not. Roy. Astron. Soc. **332** (2002) 215 [arXiv:astro-ph/0106037].

[35] A. Neronov, P. Tinyakov and I. Tkachev, arXiv:astro-ph/0402132.

[36] G. R. Blumenthal, Phys. Rev. D **1** (1970) 1596.

[37] M.J. Chodorowski, A.A. Zdziarsky and M. Sikora, Astrophys. J. **400**, 181 (1992).

[38] C. Ferrigno, P. Blasi and D. De Marco, arXiv:astro-ph/0404352.

[39] HESS: http://www.mpi-hd.mpg.de/hfm/HESS/HESS.html

[40] VERITAS: http://veritas.sao.arizona.edu/